JOC The Journal of Organic Chemistry

Article

pubs.acs.org/joc

Chiral Thiahelicene-Based Alkyl Phosphine–Borane Complexes: Synthesis, X-ray Characterization, and Theoretical and Experimental Investigations of Optical Properties

Davide Dova,[†] Silvia Cauteruccio,*[,†] Stefan Prager,[‡] Andreas Dreuw,*[,‡] Claudia Graiff,[§] and Emanuela Licandro[†]

[†]Dipartimento di Chimica, Università degli Studi di Milano, via Golgi 19, I-20133 Milan, Italy

[‡]Interdisciplinary Center for Scientific Computing, Heidelberg University, Im Neuenheimer Feld 368, 69120 Heidelberg, Germany

[§]Dipartimento di Chimica, Università degli Studi di Parma, Viale delle Scienze 17/A, 43100 Parma, Italy

Supporting Information

ABSTRACT: Chiral helical-based phosphanes are challenging and promising ligands, with a great potential for the generation of both organic and organometallic catalysts. We report here the preparation of novel chiral thiahelicene-based alkyl phosphanes, isolated and characterized as air-stable borane adducts, and the investigation of their experimental and theoretical (chir)optical properties. X-ray characterization of a mono- and a disubstituted derivative as a racemic mixture has been performed, which confirms the influence of the number and nature of substituents on the flexibility of the helix. In addition, the absolute configuration inferred from CD spectra of the two enantiomers of a diborane complex has been established from X-ray analysis. State-of-the-art quantum chemical calculations of vibrationally resolved spectra allow, for the first time, for an unambiguous assignment of the experimentally observed peaks in linear absorption and circular dichroism spectra to excited electronic states of this class of thiahelicene phosphorus derivatives.

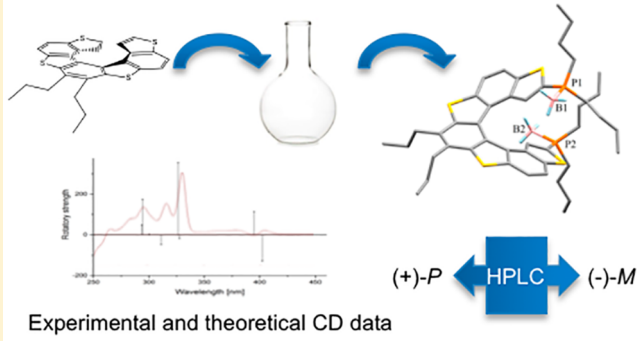

Experimental and theoretical CD data

INTRODUCTION

Helicenes belong to an intriguing class of chiral helical-shaped molecules,[1] that have nowadays reached a high degree of appeal within the scientific community on the basis of the association of synthetic challenges to manifold applications in different areas of science.[2] The configurationally fixed helical arrangement of the π system confers to helicenes a peculiar topology, and provides unique chiroptical features,[3] such as exceptionally strong circular dichroism, high optical rotation values, and several enhanced physicochemical properties. Approximate coupled cluster and density functional theory calculations proved to be a very powerful tool[4] to study circular dichroism (CD) and relevant (chir)optical properties of parent and disubstituted carbo[*n*]helicenes[3a] and diaza[6]helicenes.[3b]

Tetrathiahelicenes (7-TH), formed by thiophene and benzene rings ortho-fused in an alternating fashion, are emerging as the most popular systems,[5] on the basis of remarkable improvements in their synthesis and functionalization,[6] and on the basis of their unique electronic and optical properties suitable for applications in optoelectronics,[7] biomolecular recognition,[8] and asymmetric catalysis.[9] The effective and selective functionalization of 7-TH in the α-positions of the terminal thiophene rings allows the introduction of various types of substituents,[10] which can tune specific properties, including the flexibility of the helical skeleton and electronic properties.[11] Such a versatility and eclectic behavior is closely related to the possibility of obtaining a structural variety that still maintains the defining property of the helical structure.

In our ongoing studies on the preparation and functionalization of thiahelicenes for use in catalysis, we have recently demonstrated that 7-TH phosphorus derivatives,[9b,c,12] in which phosphorus substituents are inserted on the terminal thiophene rings, and phospha-thiahelicenes,[9a] in which a phosphorus atom is embedded in the helical structure itself, are proving to be of great interest as chiral ligands both in organometallic and organocatalyzed transformations. So far, however, only helical scaffolds with diphenyl or diaryl phosphorus groups have been reported, and only one example of helical dialkyl-substituted phosphine oxide, the 7-TH dicyclohexyl diphosphine oxide,[9b] has been studied for catalytic purposes. A more systematic investigation including different dialkylphoshine groups is therefore necessary in order to have a broader range of helical-based phosphorus compounds available to be tested in catalytic reactions. Moreover, the study of the chiroptical

Received: February 2, 2015
Published: March 16, 2015

DOI: 10.1021/acs.joc.5b00243
J. Org. Chem. 2015, 80, 3921−3928

Table 1

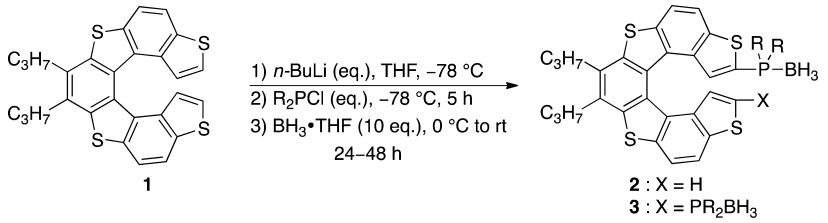

	reagents		products			
entry	*n*-BuLi/R_2PCl (equiv)	R	**2**	% yield of **2**[a]	**3**	% yield of **3**[a]
1	2/2	Cy	**2a**	62	**3a**	–
2[b]	4/4	Cy	**2a**	20	**3a**	70
3	2/2	*n*Bu	**2b**	57	**3b**	–
4	4/4	*n*Bu	**2b**	13	**3b**	61
5	1.5/2	*t*Bu	**2c**	49	**3c**	–
6	2/4	*t*Bu	**2c**	15	**3c**	78
7	1.5/2	Et	**2d**	53	**3d**	–
8	2/4	Et	**2d**	–	**3d**	76

[a]Isolated yield. [b]Literature data.[9b]

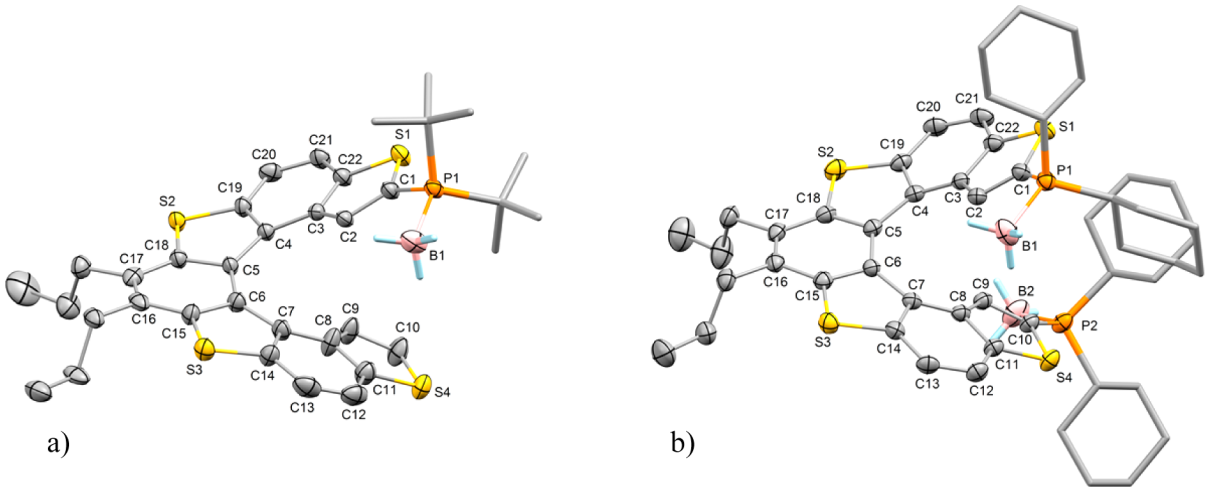

Figure 1. ORTEP diagram of (a) **2c**; (b) **3a**. Ellipsoids are shown at 30% probability level. Cy and *t*Bu moieties are depicted in stick model to avoid overlap of atoms. Hydrogen atoms and solvent molecules are omitted for clarity.

properties of 7-TH phosphorus derivatives could be essential for a deep comprehension of their intimate electronic structure and therefore of their properties. This should help in the rational design of helical phosphorus ligands for catalysis. Within this context, both theoretical calculations on chiroptical properties and tridimensional structure of this class of tetrathiahelicenes can furnish interesting and useful information.

In this article, we report the synthesis of novel 7-TH dialkyl mono- and diphosphine–borane complexes as advantageous air-stable precursors of chiral 7-TH dialkyl mono- and diphosphanes to use in catalysis. The tridimensional structure of mono- and disubstituted phosphine–borane adducts are fully established by X-ray analysis, as well as X-ray studies on the enantiopure antipodes of a diborane complex has been accomplished to unequivocally establish their absolute configuration. Finally, to achieve an in-depth understanding of the (chir)optical properties, especially the circular dichroism, of these 7-TH phosphine–borane complex systems, theoretical calculations at the approximate coupled cluster level of second order have been performed for the first time on these systems. The calculated vibrationally resolved absorption and CD spectra allow for an unambiguous assignment of the observed spectral features to individual excited electronic states.

RESULTS AND DISCUSSION

Synthesis and Characterization. On the basis of our previous experience with the preparation of tetrathiahelicene diphenylphosphane–borane adducts,[9b,c,12] we accomplished the synthesis of a set of 7-TH dialkylphosphane–borane complexes, exploiting the straightforward route described in Table 1. Thus, the reaction between the starting helicene **1** with *n*-BuLi and the appropriate amount of commercially available chlorodialkylphosphanes R_2PCl at −78 °C, including Cy_2PCl, nBu_2PCl, tBu_2PCl, and Et_2PCl, followed by the in situ addition of the complex BH_3·THF, provided mono- and disubstituted 7-TH dialkylphosphane–borane complexes **2a–d** and **3a–d**, respectively, in moderate to good yields (entries 1–8, Table 1).

In more detail, the use of 1.5 or 2 equiv of *n*-BuLi and 2 equiv of R_2PCl allowed the selective formation of monoadducts **2a–d** in 49–62% yield, without traces of the corresponding diborane complexes in the reaction mixtures (entries 1, 3, 5,

DOI: 10.1021/acs.joc.5b00243
J. Org. Chem. 2015, 80, 3921–3928

Table 2. Key Structural Parameters of Adducts 2c, 3a, and 3b Compared with Unsubstituted Helicene 1

parameters	(±)-1[11]	(±)-2c	(±)-3a	(+)-3b	(−)-3b
C2···C9 [Å]	3.153(4)	3.124(3)	3.325(3)	3.195(5)	3.226(4)
C1···C10 [Å]	4.376(5)	4.411(4)	4.693(3)	4.572(4)	4.525(4)
φ [deg][a]	53.3(1)	55.51(2)	59.41(4)	57.65(2)	57.35(2)
P···P [Å]	–	–	6.932(2)	6.391(4)	6.386(2)
P−B [Å]	–	1.918(3)	1.922(8)[b]	1.876(12)[b]	1.910(8)[b]

[a]Dihedral angle between the two terminal thiophene rings of the 7-TH skeleton. [b]Mean value.

and 7, Table 1). In these cases, about 10−40% of unreacted helicene **1** was also recovered after the chromatography purifications of the crude mixtures. On the other hand, the use of 2 or 4 equiv of *n*-BuLi and 4 equiv of R_2PCl led to the formation of the disubstituted helicenes **3a−d** in 61−78% yield, and no starting helicene **1** was recovered from the reaction mixtures (entries 2, 4, 6, and 8, Table 1). However, beside diadducts **3a−c**, a small amount (13−20%) of the corresponding monoadducts **2a−c** was also formed, presumably due to the presence of bulky alkyl moieties on the phosphorus atoms. The mono- and diadducts could be easily separated by column chromatography on silica gel. The use of more equivalents (6 or 8 equiv) of base and electrophile did not improve the yield and the selectivity in the formation of **3a−c**.

Tetrathiahelicene boranes **2a−d** (pale yellow solids) and **3a−d** (yellow solids) were fully characterized by standard analytical and spectroscopic analysis, that support the proposed structures, and unambiguously indicate the coordination of BH_3 on the phosphorus atoms bound at the alpha positions of the helical scaffold. Indeed, the IR spectra of **2** and **3** exhibited strong absorption bands at 2391−2363 cm^{-1} and at 2354−2331 cm^{-1}, which are usual B−H bond stretching frequencies of BH_3 in phosphine−borane complexes. Moreover, more diagnostic data were derived from their high-resolution ESI mass spectra, which confirm their molecular formula as sodium adduct ions, and ^{31}P NMR spectra of **2a−d** and **3a−d**, which displayed positive broad signals in the expected range from +13 to +46 ppm.

Solid-State Structure Elucidation. Single yellow crystals suitable for X-ray diffraction studies of monosubstituted adduct **2c** and disubstituted adduct **3a** were obtained from layered CH_2Cl_2/hexane, and their ORTEP diagrams along with the atomic labeling scheme are reported in Figure 1. Complexes **2c** and **3a** crystallized in the monoclinic and triclinic centrosymmetric space groups *C*2/*c* and *P*1, respectively, so both enantiomers of **2c** and **3a** are present in the crystals, as previously observed for similar 7-TH derivatives.[11] In the crystal structures of both **2c** and **3a**, the two *n*-propyl chains, linked to carbon atoms C16 and C17, are disposed on the same side with respect to the mean plane defined by the central benzene moiety. This fact allows the central benzene rings of two adjacent molecules to be stacked parallel, and the distance between their centroids is of 4.109(2) and 4.296(2) Å for **2c** and **3a**, respectively, suggesting that there are no intermolecular interactions (see Figure S3, Supporting Information). Considering the crystal packing of **2c** and **3a**, the compounds crystallized with solvent molecules (CH_2Cl_2 and hexane), which are located in the voids left by the packed molecules.

Even if the nature of the phosphine−borane substituents is different in **2c** and **3a**, a general trend for some geometrical parameters can be envisaged. The molecules tend to have shorter outer core bonds and longer inner core bonds with respect to ideal 1.39 Å (see Table S2, Supporting Information), as already found in other parent helicenes.[9c,10b,11] All seven fused rings are deviated from planarity,[13] and the dihedral angles between adjacent rings increased passing from the "external" thiophene rings to the "central" benzene ring of the helicene (see Tables S3 and S4, Supporting Information).

In Table 2 selected bond lengths, distances and angles for **2c** and **3a** are listed and compared with those of the unsubstituted helicene **1**. While there were no unusual features related to the geometry of the coordination of BH_3 to the phosphine, with P−B bond lengths of 1.918(3) for **2c** and 1.917(9) −1.926(7) Å for **3a**, some more significant distortions were found in the helical skeleton, especially related to the dihedral angle between the two terminal thiophene rings and the climb of the helix (e.g., C2···C9 and C1···C10 distances). In fact, both mono- and diborane complexes **2c** and **3a** displayed a total dihedral angle of 55.5° and 59.4°, respectively, which are notably larger than that observed in the unsubstituted helicene **1** (53.3°). Comparably, the C1····C10 distance (4.41 Å for **2c** and 4.69 Å for **3a**) was found to be higher than that of **1** (4.38 Å), with the maximum value for **3a**, bearing two bulky phosphorus moieties. For this latter compound, an intramolecular P···P distance of 6.93 Å was found, which is significantly larger than that obtained by Reetz from the X-ray crystallographic structure of the diphenyl carbo[6]helicene-based diphosphane (6.48 Å).[14] Similarly to other conjugated thiahelicenes, these results further confirm that the number and the nature of the substituents strongly influence the distortion from planarity of the helical skeleton, demonstrating the peculiar flexibility of the helical structures.

Resolution of (±)-3b and Absolute Configuration. On the basis of the air stability and good solubility in organic solvents of adducts **2** and **3**, we then decided to study the absolute configurations *P* and *M* of these systems by X-ray studies on the two enantiomers of the diborane complex (±)-**3b**, selected as model adduct. Thus, we initially separated the two enantiomers of (±)-**3b** by HPLC on chiral stationary phase, and it turned out that an efficient separation could be achieved with the Chiralpack IA column, using a ternary mobile phase (hexane/CH_2Cl_2/iso-PrOH) under isocratic conditions (see Supporting Information). The enantiopure samples of (+)-**3b** and (−)-**3b** were obtained with ee values higher than 98%, and their molar rotation values $[\phi]$ were found to be very high ((+)-**3b**: $[\alpha]_D^{22}$ +1320, $[\phi]_D^{22}$ +10596 (*c* 0.14, $CHCl_3$); (−)-**3b**: $[\alpha]_D^{22}$ −1344, $[\phi]_D^{22}$ −10790 (*c* 0.13, $CHCl_3$)), that is over three times higher than that of the unsubstituted helicene **1** ((+)-**1**: $[\alpha]_D^{20}$ +685, $[\phi]_D^{20}$ +3334 (*c* 0.19, $CHCl_3$)).[9c] Single yellow crystals suitable for X-ray analysis of both (+)-**3b** and (−)-**3b** were obtained by slow evaporation of the solvents from the corresponding HPLC eluting fractions. The enantiopure molecules crystallize, of course, in chiral space group $P2_1$. In the crystals of (+)-**3b** and (−)-**3b** there are two very similar but crystallographically independent molecules (see Figures S2 and S4, Supporting Information). The absolute configuration of the

DOI: 10.1021/acs.joc.5b00243
J. Org. Chem. 2015, 80, 3921−3928

helicity has been obtained by the refinement of the Flack parameter, which is in agreement with *P*-helicity for (+)-**3b**, and *M*-helicity for (−)-**3b**.

Regarding the structural parameters, a trend very similar to that observed in the disubstituted borane complex **3a** is evident (Table 2). Thus, the mean C1···C10 distances are 4.572(5) and 4.525(4) for (+)-**3b** and (−)-**3b**, respectively. Again, their total dihedral angle between the two terminal thiophene rings is higher [57.6° for (+)-**3b** and 57.3° for (−)-**3b**] than that of unsubstituted helicene **1** but shorter than that of **3a** (59.4°), due to the presence of more bulky cyclohexyl groups on the phosphorus atoms in **3a** with respect to the *n*butyl moieties in **3b**.

Chiroptical Properties and Theoretical Calculations. The lack of an in-depth study of the chiroptical properties of 7-TH phosphorus derivatives prompted us to examine the CD spectra of the enantiopure adducts (+)-**3b** and (−)-**3b**, through both experimental and computational studies. The experimental CD spectra of (+)-**3b** and (−)-**3b** are reported in Figure 2

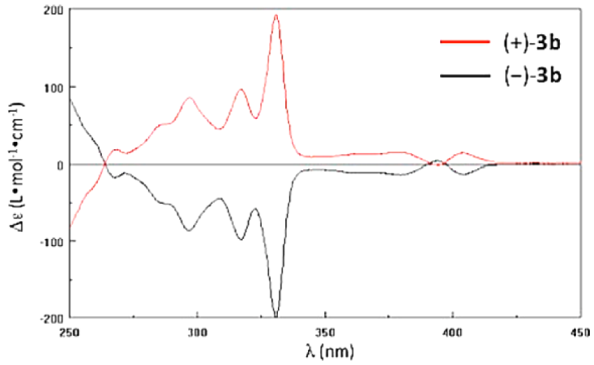

Figure 2. Experimental CD spectra of (+)-**3b** and (−)-**3b** ($CHCl_3$, 10^{-4} M).

and display a strong positive and negative CD band (β band) around 300−340 nm for (+)-**3b**, and (−)-**3b**, respectively. Since it is commonly accepted that the sign of the most intense CD band (β band) is representative of the absolute configuration of the helicene, with a positive (negative) band corresponding to *P* (*M*) helicity, the *P* helicity can be attributed to the enantiomer (+)-**3b** and vice versa for (−)-**3b**, in perfect agreement with the results obtained from X-ray studies.

As first step of our theoretical investigation of the optical properties of the two enantiomers of **3b**, the equilibrium ground-state structures of (+)-**3b** and (−)-**3b** have been separately optimized at DFT/ωB97XD/cc-pVDZ level of theory,[15] and the calculated geometrical parameters of the equilibrium structures agree very favorably with the obtained crystal structures (see Table S5, Supporting Information). Turning to the excited-state properties of **3b**, we calculated the eight energetically lowest excited singlet states at the optimized ground-state equilibrium geometry using RI-CC2/cc-pVDZ (see Table S6, Supporting Information). For comparison of the calculated excitation energies with the experimentally determined absorption spectrum, their values are shifted to lower energies by −0.325 eV, accounting for systematic errors in the calculation stemming from the approximate level of computation and the lack of solvation effects. The energy shift has been chosen such that the first excitation energy matches the first absorption band. As can be seen in Figure 3, an overall very good agreement of the computed excitation energies at the RI-CC2 level of theory and the experimental absorption spectrum is achieved.

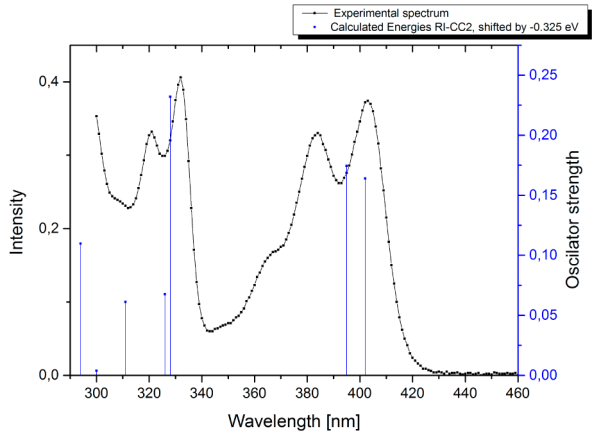

Figure 3. Excitation energies (shifted by −0.325 eV, see text) and oscillator strengths of the eight lowest electronically excited states calculated at the RI-CC2/cc-pVDZ level of theory compared to the experimental spectrum.

Analyzing the individual excited states in detail, the first electronically excited state (S_1) is mainly characterized by a HOMO-1 to LUMO transition (80.3%), and the second excited state (S_2) is characterized as HOMO to LUMO transition (89.6%). Both states could contribute to the first experimental absorption band at 400 nm wavelengths. The third excited state S_3, characterized by several lower-contributing orbital transitions (HOMO−2 to LUMO 57.4%, HOMO to LUMO+1 12.3%, HOMO−1 to LUMO 6.0%, HOMO−1 to LUMO+2 4.0%) corresponds most probably to the absorption band at 320 nm wavelengths. However, it remains unclear whether the second experimental band at 380 nm wavelengths corresponds to the S_2 or to vibrational progression of the S_1 state. To elaborate this question, vibrationally resolved absorption spectra[16] of the $S_0 \rightarrow S_1$ and the $S_0 \rightarrow S_2$ transitions were calculated at TDDFT/ωB97XD/cc-pVDZ level of theory (for technical details, see Supporting Information). The calculated vibrationally resolved peaks are analogously shifted to match the excitation energy difference of the states as calculated at the RI-CC2/cc-pVDZ level of theory. Thereby vibrationally resolved absorption spectra are obtained, for which the electronic contributions are calculated at high RI-CC2 level and the vibrational contributions stem from lower-level TDDFT calculations. For comparison with the experimental absorption spectrum, the computed vibrationally resolved spectra of S_1 and S_2 have been added (Figure 4).

As can be readily seen, the vibrationally resolved spectrum of state S_2 exhibits a much weaker intensity than the spectrum of state S_1, although both have similar oscillator strengths. Obviously, the band of S_2 is much broader than the one of S_1, and many vibrational modes contribute to the spectrum. It is clear now that S_1 dominates the first band of the spectrum, while S_2 contributes only marginally. The vibrational progression of the sum of the $S_0 \rightarrow S_1$ and $S_0 \rightarrow S_2$ transitions (Figure 4) corresponds very nicely to the observed peaks at 405, 385, and 365 nm absorption wavelength in the experimental spectrum. This also explains the mirror-like emission and excitation spectra of several tetrathiahelicenes.[12] Since the S_1 state responsible for the first absorption band is

DOI: 10.1021/acs.joc.5b00243
J. Org. Chem. 2015, 80, 3921−3928

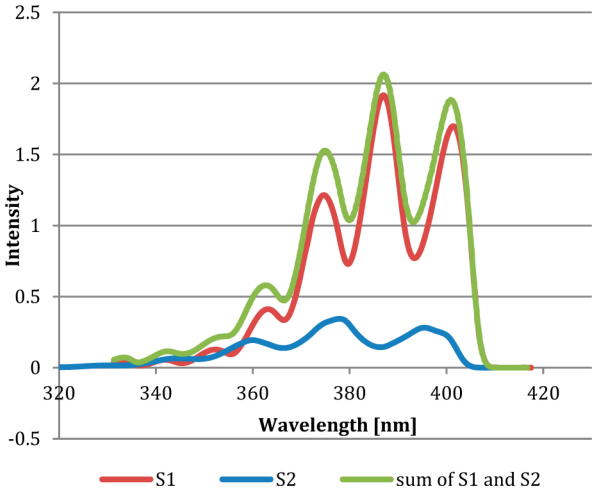

Figure 4. Vibrationally resolved absorption spectra of states S_1 and S_2 of **3b** and the sum of both spectra contributing to the first band of the experimental absorption spectrum.

located strictly at the central helicene part, which is identical in all 7-TH-analogues, one can expect these compounds to exhibit very similar spectra. The observed negligible variations are then due to electronic and steric effects of side groups or heavy atoms.

Rotatory strengths have been calculated at the RI-CC2/cc-pVDZ level of theory, which are required for the simulation of CD spectra (Figure 5, and Table S6, Supporting Information).

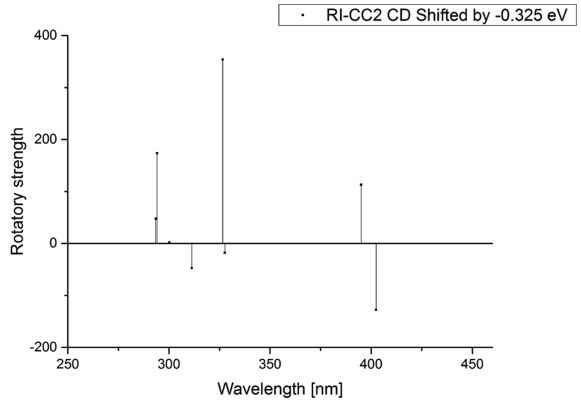

Figure 5. Simulated CD spectrum of (+)-**3b** using the eight energetically lowest excited states computed at RI-CC2/cc-pVDZ level of theory.

The first and second excited states show very similar values for the rotatory strength *R* but with opposite sign. Since they are also very close in energy, they cancel each other almost completely, which can be seen in the experimental CD spectrum. Also, taking the computed vibrational broadening of these states into account explains the broad flat region from 420 to 350 nm wavelength in the experimental CD spectrum. S_3 shows only a very small rotatory strength although it exhibits the largest oscillator strength. In contrast, S_4 has the largest rotatory strength and can thus be assigned to the large band in the experimental spectrum at 330 nm with a vibrational overtone at 315 nm. The next band at 295 nm corresponds most likely to S_7. Of course, the simulated CD spectrum of (−)-**3b** is the mirror image of the one of (+)-**3b** inflected at the wavelength axis.

CONCLUSIONS

In summary, in this paper we have described the synthesis of novel air-stable tetrathia[7]helicene alkyl phosphine−borane complexes **2a−d** and **3b−d**, in which two alkyl groups are present on the phosphorus atom directly bound to the helix. These compounds have been obtained in moderate to good yields, by a selective and straightforward protocol starting from the unsubstituted helicene **1**, commercially available chlorodialkylphosphanes, and BH_3·THF complex. The complete spectroscopic and analytical characterization of **2a−d** and **3b−d** have been accomplished, along with the full elucidation of the tridimensional structures of racemic **2d** and **3a**, selected as model mono- and diborane complexes, which have demonstrated that the geometrical features and flexibility of the helix of these thiahelicene-based systems are strongly influenced by the nature and number of substituents on the helical skeleton. Moreover, X-ray studies on the enantiopure disubstituted phosphine−boranes (+)-**3c** and (−)-**3c** allowed us to confirm their absolute configuration and unequivocally assign the *P* configuration for the (+) enantiomer and the *M* configuration for the (−) enantiomer for this class of 7-TH phosphorus derivatives. These experimental results are in perfect agreement with those obtained by theoretical correlation on the basis of their experimental CD spectra.

Circular dichroism and relevant chiroptical properties of enantiomers (+)-**3c** and (−)-**3c** were also investigated by state-of-the-art approximate coupled cluster and density functional theory calculations, results of which were compared with the corresponding experimental data. The theoretical calculations at RI-CC2 level accurately reproduced the experimental UV−vis and CD spectra. The analysis of the contributing excited electronic states revealed that absorption spectra can be expected to be very similar for thiahelicene-based systems, while the low-energy region of the CD spectrum is dominated by a compensation of bands with opposite sign. Hence, CD spectra are expected to be more sensitive to small differences in the structures of thiahelicenes, which modulate the relative energetic position of the S_1 and S_2 states.

This is the first combined theoretical and experimental study on the structural and chiroptical properties of tetrathiahelicene-based phosphine−borane complexes, which represents a valuable platform to design new chiral alkyl phosphorus ligands to be used in catalysis. To fully elucidate other useful properties, such as the electronic and steric features of the free phosphines and the corresponding phosphine oxides obtained by the borane complexes described in this work, further studies, including electrochemical investigations, are in progress in our laboratory.

EXPERIMENTAL SECTION

General Methods. All reactions were performed under a positive argon atmosphere using standard Schlenk and vacuum-line techniques. All glassware was flame-dried and cooled under vacuum before use. Anhydrous THF was purged with argon prior to use. Solutions of *n*-BuLi (1.6 M in hexane) were purchased from Aldrich and titrated prior to use. BH_3·THF complex (1 M in THF), Cy_2PCl, Bu_2PCl, *t*-Bu_2PCl, and Et_2PCl were purchased from Aldrich and used as received. Compounds **1**[6d] and **3a**[9b] were prepared and characterized as previously reported. Thin-layer chromatography (TLC) was performed with Merck silica gel 60 F254 precoated plates, and visualized with UV (254 and 366 nm). Flash chromatography was performed with Merck silica gel 60 (230−400 mesh). ^1H, $^{13}C\{^1H\}$, and $^{31}P\{^1H\}$ NMR spectra were recorded in $CDCl_3$ at 25 °C using 300 MHz NMR spectrometer. Chemical shifts were reported relative to residual

DOI: 10.1021/acs.joc.5b00243
J. Org. Chem. 2015, 80, 3921−3928

protonated solvent resonances (δ H 7.26 ppm, δ C 77.16 ppm), or the external standard H_3PO_4 ($^{31}P\{^1H\}$). High-resolution mass spectra (HRMS) were recorded by Fourier transform ion cyclotron resonance mass spectrometry (ICR-FTMS).

Theoretical Calculations. For the theoretical investigation on the optical properties of the two enantiomers of **3b**, time-dependent density functional theory (TD-DFT)[17] and approximate coupled-cluster theory of second-order (CC2)[18] in combination with the basis set cc-pVDZ[15b] were employed. In addition, for CC2, the "resolution of the identity" (RI) approximation[19] was applied with the corresponding auxiliary basis set aux-cc-pVDZ. For the underlying ground-state DFT and excited-state TD-DFT calculations, the exchange-correlation (xc)-functional ωB97XD[15a] was used. For the RI-CC2 calculations, Turbomole 6.3.1[20] was employed, while for DFT and TD-DFT calculations, the Gaussian 09 Rev. D.01[21] program package was used.

General Procedure for the Synthesis of Phosphane−Borane Complexes 2a−d and 3b−d. A solution of *n*-BuLi (0.25 or 0.5 mL, 0.40 or 0.80 mmol) was added dropwise to a stirred solution of **1** (100 mg, 0.20 mmol) in dry THF (10 mL) at −78 °C under an argon atmosphere. The solution was stirred for 20 min at −78 °C, heated to room temperature for 20 min, and then cooled back to −78 °C. To the cooled reaction solution was added the appropriate chlorodialkylphosphine (0.40 or 0.80 mmol), and the mixture was stirred for 20 min at −78 °C and for 5 h at rt. The suspension was cooled back to 0 °C and treated with a solution of BH_3·THF complex (2.0 mL, 2.0 mmol). The yellow suspension was stirred at room temperature for 24−48 h. Upon completion, the reaction mixture was diluted with CH_2Cl_2 (10 mL) and slowly added to a saturated aqueous NH_4Cl solution (50 mL). The aqueous phase was extracted with CH_2Cl_2 (×3). The organic layer was washed with brine (×3), dried over anhydrous Na_2SO_4, filtered, and concentrated under reduced pressure. Purification of the residue was accomplished by column chromatography using silica gel with hexanes and DCM as the eluent.

Monoborane Adduct ***2a***. Purification was accomplished with a 7/3 hexanes/DCM solvent mixture, which yielded **2a** (89 mg, 62%) as a yellow solid: mp 245−248 °C; ^{1}H NMR (300 MHz, $CDCl_3$) δ 8.07−7.94 (m, 4H), 7.43 (d, $^3J_{(H,H)}$ = 7.7 Hz, 1H), 6.90 (d, $^3J_{(H,H)}$ = 5.5 Hz, 1H), 6.79 (d, $^3J_{(H,H)}$ = 5.5 Hz, 1H), 3.16−3.08 (m, 4H), 1.88−1.64 (m, 15H), 1.19−1.12 (m, 17H); $^{13}C\{^1H\}$ NMR (75 MHz, $CDCl_3$) δ 140.8 (C), 140.2 (C), 140.0 (C), 137.7 (C), 136.8 (d, $^2J_{(C,P)}$ = 10.6 Hz, CH), 136.7 (C), 136.5 (C), 135.9 (d, $^3J_{(C,P)}$ = 11.6 Hz, Cq), 135.6 (C), 132.9 (C), 132.0 (d, $^1J_{(C,P)}$ = 56.8 Hz, C), 128.7 (C), 127.9 (C), 126.6 (C), 126.0 (C), 125.3 (CH), 124.3 (CH), 121.6 (CH), 120.6 (CH), 120.3 (CH), 119.3 (CH), 34.6 (CH_2), 34.5 (CH_2), 33.3 (d, $^1J_{(C,P)}$ = 29.5 Hz, CH), 32.8 (d, $^1J_{(C,P)}$ = 29.5 Hz, CH), 26.9 (CH_2), 26.8 (CH_2), 26.7 (CH_2), 26.6 (CH_2), 26.5 (CH_2), 26.4 (CH_2), 26.3 (CH_2), 26.2 (CH_2), 26.1 (CH_2), 25.9 (CH_2), 23.4 (2 CH_2), 14.9 (CH_3), 14.8 (CH_3); $^{31}P\{^1H\}$ NMR (121 MHz, $CDCl_3$) δ 25.6 (br s); IR (neat) ν 2370, 2332 cm^{-1} (B−H bond stretching); UV−vis (DCM) λ_{max} (ε) 292 (23600), 318 (18300), 326 (16400), 379 (17800), 397 nm (19400 mol^{-1}dm^{3}cm^{-1}); HRMS (ESI, positive mode) m/z $[C_{40}H_{46}S_4PBNa]^+$ calcd for $C_{40}H_{46}S_4PBNa$ 719.2205, found 719.2210.

Monoborane Adduct ***2b***. Purification was accomplished with a 7/3 hexanes/DCM solvent mixture, which yielded **2b** (75 mg, 57%) as a yellow solid: mp 198−200 °C; ^{1}H NMR (300 MHz, $CDCl_3$) δ 8.05−7.96 (m, 4H), 7.23 (d, $^3J_{(H,P)}$ = 7.3 Hz, 1H), 6.91 (d, $^3J_{(H,H)}$ = 5.6 Hz, 1H), 6.75 (d, $^3J_{(H,H)}$ = 5.6 Hz, 1H), 3.20−3.09 (m, 4H), 1.90−1.83 (m, 4H), 1.49−1.38 (m, 4H), 1.31−1.20 (m, 6H), 1.18−1.14 (m, 8H), 0.87−0.80 (m, 6H) ppm; $^{13}C\{^1H\}$ NMR (75 MHz, $CDCl_3$) δ 140.7 (2C), 140.2 (2C), 137.2 (C), 136.6 (d, $^4J_{(C,P)}$ =2.2 Hz, C), 136.0 (d, $^3J_{(C,P)}$ = 10.8 Hz, C), 135.8 (C), 133.5 (d, $^2J_{(C,P)}$= 7.5 Hz, CH), 132.9 (C), 132.4 (C), 132.0 (C), 131.4 (C), 129.7 (d, $^1J_{(C,P)}$ = 48 Hz, C), 128.4 (C), 128.0 (C), 125.5 (CH), 124.3 (CH), 121.3 (CH), 120.6 (CH), 120.5 (CH), 119.2 (CH), 34.5 ($2CH_2$), 26.4 (d, $^1J_{(C,P)}$= 35.5 Hz, CH_2,), 26.2 (d, $^1J_{(C,P)}$ = 36.0 Hz, CH_2), 25.0 ($2CH_2$), 24.3 (d, $^2J_{(C,P)}$ = 14.0 Hz, CH_2), 24.2 (d, $^2J_{(C,P)}$ = 13.7 Hz, CH_2), 23.4 ($2CH_2$), 14.8 ($2CH_3$), 13.7 (CH_3), 13.6 (CH_3) ppm; $^{31}P\{^1H\}$ NMR (121 MHz, $CDCl_3$)δ 13.4 (br s) ppm; IR (neat) ν 2386, 2340 cm^{-1} (B−H bond stretching); UV−vis (DCM) λ_{max} (ε) 228, 243, 292 (28900), 318 (23500), 326 (20800), 378 (23000), 398 nm (25800 mol^{-1}dm^{3}cm^{-1}); HRMS (ESI, positive mode) m/z $[C_{36}H_{42}S_4PBNa]^+$ calcd for $C_{36}H_{42}S_4PBNa$ 667.1892, found 667.1892.

Diborane Adduct ***3b***. Purification was accomplished with a 1/1 hexanes/DCM solvent mixture, which yielded **3b** (101 mg, 71%) as a yellow solid: mp 215 °C; ^{1}H NMR (300 MHz, $CDCl_3$) δ 8.09−8.02 (m, 4H), 7.18 (d, $^3J_{(H,P)}$ = 7.3 Hz, 2H), 3.18−3.06 (m, 4H), 1.95−1.81 (m, 4H), 1.67−1.56 (m, 2H), 1.47−1.42 (m, 6H), 1.41−1.14 (m, 22H), 0.87−0.82 (m, 12H) ppm; $^{13}C\{^1H\}$ NMR (75 MHz, $CDCl_3$) δ 141.1 (C), 140.4 (C), 136.9 (C), 135.6 (d, $^3J_{(C,P)}$ = 10.6 Hz, C), 133.6 (d, $^2J_{(C,P)}$ = 7.9 Hz, CH), 132.9 (C), 131.6 (C), 130.0 (d, $^1J_{(C,P)}$ = 48 Hz, C), 127.9 (C), 120.9 (CH), 120.8 (CH), 34.5 (CH_2), 27.0 (d, $^1J_{(C,P)}$ = 35.6 Hz, $2CH_2$), 25.7 (d, $^1J_{(C,P)}$ = 36.0 Hz, $2CH_2$), 25.0 ($2CH_2$), 24.9 ($2CH_2$), 24.3 (d, $^2J_{(C,P)}$ = 14.0 Hz, $2CH_2$), 24.2 (d, ^2J(C,P) = 13.7 Hz, $2CH_2$), 23.4 (CH_2), 14.8 (CH_3) 13.7 ($2CH_3$), 13.6 ($2CH_3$) ppm; $^{31}P\{^1H\}$ NMR (121 MHz, $CDCl_3$) δ 13.35 (br s) ppm; IR (neat) ν 2389, 2343 cm^{-1} (B−H bond stretching); UV−vis (DCM) λ_{max} (ε) 227, 249, 292 (29600), 321 (23100), 332 (28200), 384 (22900), 404 nm (25700 mol^{-1}dm^{3}cm^{-1}); HRMS (ESI, positive mode): m/z $[C_{44}H_{62}S_4P_2B_2Na^+]$ calcd for $C_{44}H_{62}S_4P_2B_2Na$ 825.3288; found 825.3306.

Monoborane Adduct ***2c***. Purification was accomplished with a 7/3 hexanes/DCM solvent mixture, which yielded **2c** (65 mg, 49%) as a yellow solid: mp 171−173 °C; ^{1}H NMR (300 MHz, $CDCl_3$) δ 8.04−7.96 (m, 4H), 7.66 (d, $^3J_{(H,P)}$ = 7.1 Hz, 1H), 6.93 (d, $^3J_{(H,H)}$ = 5.6 Hz, 1H), 6.86 (d, $^3J_{(H,H)}$ = 5.6 Hz, 1H), 3.15−3.09 (m, 4H), 1.88−1.85 (m, 4H), 1.17 (m, 6H, CH_3), 1.14 (s, 6H), 1.09 (s, 4H), 0.99 (s, 4H), 0.94 ppm (s, 4H); $^{13}C\{^1H\}$ NMR (75 MHz, $CDCl_3$) δ = 140.8 (C), 140.1 (C), 139.8 (C), 137.9 (C), 137.2 (d, $^2J_{(C,P)}$= 7.5 Hz, CH), 136.6 (C), 136.3 (C), 135.7 (d, $^3J_{(C,P)}$= 10.5 Hz, C), 135.5 (C), 132.7 (C), 131.83 (d, $^1J_{(C,P)}$= 48.7 Hz, C), 131.81 (C), 131.5 (C), 128.5 (C), 127.7 (C), 126.5 (d, $^1J_{(C,P)}$= 38.3 Hz, C), 124.9 (CH), 124.6 (CH), 121.3 (CH), 120.5 (CH), 119.9 (CH), 119.2 (CH), 34.4 (CH_2), 34.3 (CH_2), 33.3 (d, $^1J_{(C,P)}$= 27 Hz, C), 32.9 (d, $^1J_{(C,P)}$= 28.7 Hz, C), 28.5 ($3CH_3$), 28.3 ($3CH_3$), 23.3 ($2CH_2$), 14.73 (CH_3), 14.66 (CH_3) ppm; $^{31}P\{^1H\}$ NMR (121 MHz, CDCl3) δ 45.76 (br s) ppm; IR (neat): ν = 2384, 2354 (B−H bond stretching) cm^{-1}; UV−vis (DCM) λ_{max} (ε) = 228, 292 (20900), 318 (16000), 327 (15100), 378 (16200), 397 nm (17800 mol^{-1} dm^3 cm^{-1}); HRMS (ESI, positive mode): m/z $[C_{36}H_{42}S_4PBNa^+]$ calcd for $C_{36}H_{42}S_4PBNa$ 667.1892; found 667.1898.

Diborane Adduct ***3c***. Purification was accomplished with a 1/1 hexanes/DCM solvent mixture, which yielded **3c** (129 mg, 78%) as a yellow solid: mp 294−296 °C; ^{1}H NMR (300 MHz, $CDCl_3$): δ = 8.05 (d, $^3J_{(H,H)}$ = 8.7 Hz, 2H), 7.98 (d, $^3J_{(H,H)}$ = 8.7 Hz, 2H), 7.65 (d, $^3J_{(H,P)}$ = 6.8 Hz, 2H), 3.15−3.06 (m, 4H), 1.90−1.85 (m, 4H), 1.17 (t, $^2J_{(H,H)}$ = 7.3 Hz, 6H), 1.07−0.93 (m, 36H) ppm; $^{13}C\{^1H\}$ NMR (121 MHz, $CDCl_3$) δ = 142.1 (C), 140.4 (C), 137.0 (C), 136.2 (d, $^2J_{(C,P)}$ = 6.8 Hz, CH), 135.5 (d, $^3J_{(C,P)}$ = 10.5 Hz, C), 132.7 (C), 132.0 (C), 128.0 (C), 127.0 (d, $^1J_{(C,P)}$ = 38.3 Hz, C), 121.0 (CH), 120.7 (CH), 34.5 (CH_2), 33.3 (d, $^1J_{(C,P)}$ = 26.3 Hz, CH_2), 33.0 (d, $^1J_{(C,P)}$ = 26.3 Hz, CH_2), 28.6 (CH_3), 28.4 (CH_3), 23.5 (CH_2), 14.9 (CH_3) ppm; $^{31}P\{^1H\}$ NMR (121 MHz, $CDCl_3$) δ = 45.95 (br s) ppm; IR (neat): ν = 2391 (B−H bond stretching), 2352 (B−H bond stretching) cm^{-1}; UV−vis (DCM) λ_{max} (ε) = 259, 295 (34700), 321 (26000), 333 (36900), 384 (26600), 403 nm (29400 mol^{-1} dm^3 cm^{-1}); HRMS (ESI, positive mode): m/z $[C_{44}H_{62}S_4P_2B_2Na^+]$ calcd for $C_{44}H_{62}S_4P_2B_2Na$ 825.3288; found 825.3296.

Monoborane Adduct ***2d***. Purification was accomplished with a 7/3 hexanes/DCM solvent mixture, which yielded **2d** (70 mg, 57%) as a yellow solid: mp 170−172 °C; ^{1}H NMR (300 MHz, $CDCl_3$) δ 8.03−7.96 (m, 4H), 7.27 (d, $^3J_{(H,H)}$ = 6.4 Hz, 1H), 6.91 (d, $^3J_{(H,H)}$ = 5.2 Hz, 1H), 6.75 (d, $^3J_{(H,H)}$ = 5.2 Hz, 1H), 3.14−3.12 (m, 4H), 1.88−1.86 (m, 4H), 1.51−1.49 (m, 4H), 1.17 (m, 6H), 0.94−0.84 (m, 6H); $^{13}C\{^1H\}$ NMR (75 MHz, $CDCl_3$) δ 140.7 (2C), 140.2 (2C), 137.3 (C), 136.6 (C), 136.1 (d, $^3J_{(C,P)}$ = 10.3 Hz, C), 135.7 (C), 134.0 (d, $^2J_{(C,P)}$ = 7.8 Hz, CH), 132.9 (C), 132.4 (C), 132.0 (C), 131.4 (C), 128.7 (d, $^1J_{(C,P)}$ = 48.0 Hz, C), 128.4 (C), 127.9 (C), 125.4 (CH), 124.3 (CH), 121.2 (CH), 120.6 (CH), 120.4 (CH), 119.3 (CH), 34.5 ($2CH_2$), 23.4 ($2CH_2$), 19.7 (d, $^1J_{(C,P)}$ = 36.6 Hz, CH_2), 19.3 (d, $^1J_{(C,P)}$ = 36.9 Hz, CH_2), 14.8 ($2CH_3$), 7.1 ($2CH_3$); $^{31}P\{^1H\}$ NMR (121 MHz, $CDCl_3$) δ

DOI: 10.1021/acs.joc.5b00243
J. Org. Chem. 2015, 80, 3921−3928

18.5 (br s) ppm; IR (neat) ν 2364, 2331 cm^{-1} (B−H bond stretching); UV−vis (DCM) λ_{max} (ε) = 263, 292 (30300), 318 (24000), 333 (36900), 378 (23600), 398 nm (25600 mol^{-1} dm^3 cm^{-1}); HRMS (ESI, positive mode) m/z $[C_{32}H_{34}S_4PBNa]^+$ calcd for $C_{32}H_{34}S_4PBNa$ 611.1266, found 611.1264.

Diborane Adduct ***3d***. Purification was accomplished with a 1/1 hexanes/DCM solvent mixture, which yielded **3d** (106 mg, 76%) as a yellow solid: mp 168−170 °C; ^1H NMR (300 MHz, $CDCl_3$) δ 8.08−8.01 (m, 4H), 7.22 (d, $^3J_{(H,H)}$ = 7.4 Hz, 2H), 3.17−3.08 (m, 4H), 1.87−1.84 (m, 4H), 1.63−1.56 (m, 4H), 1.49−1.40 (m, 4H), 1.18−1.13 (m, 6H), 0.98−0.79 (m, 12H); $^{13}C\{^1H\}$ NMR (75 MHz, $CDCl_3$) δ 141.4 (C), 140.4 (C), 136.9 (C), 135.6 (d, $^3J_{(C,P)}$ = 10.7 Hz, C), 134.1 (d, $^2J_{(C,P)}$ = 8.6 Hz, CH), 132.9 (C), 131.6 (C), 129.0 (d, $^1J_{(C,P)}$ = 47.0 Hz, C), 127.8 (C), 120.9 (CH), 120.8 (CH), 34.5 (CH_2), 23.4 (CH_2), 20.0 (d, $^1J_{(C,P)}$ = 36.7 Hz, CH_2), 18.8 (d, $^1J_{(C,P)}$ = 36.9 Hz, CH_2), 14.8 (CH_3), 7.3 (CH_3), 7.0 (CH_3); $^{31}P\{^1H\}$ NMR (121 MHz, $CDCl_3$) δ 18.5 (br s) ppm; IR (neat) ν 2365, 2335 cm^{-1} (B−H bond stretching); UV−vis (DCM) λ_{max} (ε) = 252, 292 (27700), 320 (21000), 332 (27400), 384 (21300), 403 nm (24300 $mol^{-1}dm^3cm^{-1}$); HRMS (ESI, positive mode) m/z $[C_{36}H_{46}S_4P_2B_2Na]^+$ calcd for $C_{36}H_{46}S_4P_2B_2Na$ 713.2036, found 713.2047.

■ ASSOCIATED CONTENT

Ⓢ Supporting Information

^1H and ^{13}C NMR spectra of **2a−d** and **3b−d**, experimental UV−vis absorption spectra of **1**, **2a−d**, and **3a−d**, and supplementary experimental, crystallographic, and computational data. This material is available free of charge via the Internet at http://pubs.acs.org.

■ AUTHOR INFORMATION

Corresponding Authors

*E-mail: silvia.cauteruccio@unimi.it.

*E-mail: dreuw@uni-heidelberg.de.

Notes

The authors declare no competing financial interest.

■ ACKNOWLEDGMENTS

D.D. and S.C. thank the Università degli Studi di Milano for the Ph.D. and postdoctoral fellowship. S.P. is a member of the Heidelberg Graduate School for Mathematical and Computational Methods for the Sciences (GSC 220) funded by the Deutsche Forschungsgemeinschaft DFG.

■ REFERENCES

(1) (a) Hoffmann, N. *J. Photochem. Photobiol., C* **2014**, *19*, 1−19. (b) Gingras, M. *Chem. Soc. Rev.* **2013**, *42*, 968−1006. (c) Gingras, M.; Felix, G.; Peresutti, R. *Chem. Soc. Rev.* **2013**, *42*, 1007−50. (d) Shen, Y.; Chen, C.-F. *Chem. Rev.* **2012**, *112*, 1463−535.

(2) (a) Narcis, M. J.; Takenaka, N. *Eur. J. Org. Chem.* **2014**, 21−34. (b) Gingras, M. *Chem. Soc. Rev.* **2013**, *42*, 1051−95.

(3) (a) Nakai, Y.; Mori, T.; Inoue, Y. *J. Phys. Chem. A* **2012**, *116*, 7372−85. (b) Nakai, Y.; Mori, T.; Inoue, Y. *J. Phys. Chem. A* **2013**, *117*, 83−93.

(4) Friese, D. H.; Hattig, C. *Phys. Chem. Chem. Phys.* **2014**, *16*, 5942−51.

(5) Collins, S. K.; Vachon, M. P. *Org. Biomol. Chem.* **2006**, *4*, 2518−24.

(6) (a) Waghray, D.; de Vet, C.; Karypidou, K.; Dehaen, W. *J. Org. Chem.* **2013**, *78*, 11147−54. (b) Waghray, D.; Dehaen, W. *Org. Lett.* **2013**, *15*, 2910−13. (c) Waghray, D.; Nulens, W.; Dehaen, W. *Org. Lett.* **2011**, *13*, 5516−19. (d) Licandro, E.; Rigamonti, C.; Ticozzelli, M. T.; Monteforte, M.; Baldoli, C.; Giannini, C.; Maiorana, S. *Synthesis* **2006**, 3670−78. (e) Baldoli, C.; Bossi, A.; Giannini, C.; Licandro, E.; Maiorana, S.; Perdicchia, D.; Schiavo, M. *Synlett* **2005**, 1137−41. (f) Maiorana, S.; Papagni, A.; Licandro, E.; Annunziata, R.; Paravidino, P.; Perdicchia, D.; Giannini, C.; Bencini, M.; Clays, K.; Persoons, A. *Tetrahedron* **2003**, *59*, 6481−88.

(7) (a) Rose-Munch, F.; Li, M.; Rose, E.; Daran, J. C.; Bossi, A.; Licandro, E.; Mussini, P. R. *Organometallics* **2012**, *31*, 92−104. (b) Kim, C.; Marks, T. J.; Facchetti, A.; Schiavo, M.; Bossi, A.; Maiorana, S.; Licandro, E.; Todescato, F.; Toffanin, S.; Muccini, M.; Graiff, C.; Tiripicchio, A. *Org. Electron.* **2009**, *10*, 1511−20. (c) Bossi, A.; Licandro, E.; Maiorana, S.; Rigamonti, C.; Righetto, S.; Stephenson, G. R.; Spassova, M.; Botek, E.; Champagne, B. *J. Phys. Chem. C* **2008**, *112*, 7900−07. (d) Champagne, B.; André, J.-M.; Botek, E.; Licandro, E.; Maiorana, S.; Bossi, A.; Clays, K.; Persoons, A. *ChemPhysChem* **2004**, *5*, 1438−42.

(8) (a) Cauteruccio, S.; Bartoli, C.; Carrara, C.; Dova, D.; Errico, C.; Ciampi, G.; Dinucci, D.; Licandro, E.; Chiellini, F. *Chem. Plus. Chem.* **2014**, *80*, 490−3. (b) Shinohara, K.; Sannohe, Y.; Kaieda, S.; Tanaka, K.; Osuga, H.; Tahara, H.; Xu, Y.; Kawase, T.; Bando, T.; Sugiyama, H. *J. Am. Chem. Soc.* **2010**, *132*, 3778−82. (c) Xu, Y.; Zhang, Y. X.; Sugiyama, H.; Umano, T.; Osuga, H.; Tanaka, K. *J. Am. Chem. Soc.* **2004**, *126*, 6566−7.

(9) (a) Aillard, P.; Voituriez, A.; Dova, D.; Cauteruccio, S.; Licandro, E.; Marinetti, A. *Chem.—Eur. J.* **2014**, *20*, 12373−76. (b) Cauteruccio, S.; Dova, D.; Benaglia, M.; Genoni, A.; Orlandi, M.; Licandro, E. *Eur. J. Org. Chem.* **2014**, 2694−702. (c) Monteforte, M.; Cauteruccio, S.; Maiorana, S.; Benincori, T.; Forni, A.; Raimondi, L.; Graiff, C.; Tiripicchio, A.; Stephenson, G. R.; Licandro, E. *Eur. J. Org. Chem.* **2011**, 5649−58. (d) Kawasaki, T.; Suzuki, K.; Licandro, E.; Bossi, A.; Maiorana, S.; Soai, K. *Tetrahedron: Asymmetry* **2006**, *17*, 2050−53.

(10) (a) Rigamonti, C.; Ticozzelli, M. T.; Bossi, A.; Licandro, E.; Giannini, C.; Maiorana, S. *Heterocycles* **2008**, *76*, 1439−70. (b) Bossi, A.; Maiorana, S.; Graiff, C.; Tiripicchio, A.; Licandro, E. *Eur. J. Org. Chem.* **2007**, 4499−509.

(11) Bossi, A.; Falciola, L.; Graiff, C.; Maiorana, S.; Rigamonti, C.; Tiripicchio, A.; Licandro, E.; Mussini, P. R. *Electrochim. Acta* **2009**, *54*, 5083−97.

(12) Cauteruccio, S.; Loos, A.; Bossi, A.; Blanco Jaimes, M. C.; Dova, D.; Rominger, F.; Prager, S.; Dreuw, A.; Licandro, E.; Hashmi, A. S. K. *Inorg. Chem.* **2013**, *52*, 7995−8004.

(13) Nakagawa, H.; Obata, A.; Yamada, K.; Kawazura, H. *J. Chem. Soc., Perkin Trans. 2* **1985**, 1899−903.

(14) Reetz, M. T.; Beuttenmüller, E. W.; Goddard, R. *Tetrahedron Lett.* **1997**, *38*, 3211−14.

(15) (a) Chai, J.-D.; Head-Gordon, M. *Phys. Chem. Chem. Phys.* **2008**, *10*, 6615−20. (b) Dunning, T. H. *J. Chem. Phys.* **1989**, *90*, 1007−23.

(16) Barone, V.; Bloino, J.; Biczysko, M.; Santoro, F. *J. Chem. Theory Comput.* **2009**, *5*, 540−54.

(17) Parr, R. G.; Yang, W. *Density-Functional Theory of Atoms and Molecules*; Oxford Science Publication: New York, 1989.

(18) Christiansen, O.; Koch, H.; Jørgensen, P. *Chem. Phys. Lett.* **1995**, *243*, 409−18.

(19) (a) Hättig, C.; Weigend, F. *J. Chem. Phys.* **2000**, *113*, 5154−61. (b) Eichkorn, K.; Treutler, O.; Ohm, H.; Haser, M.; Ahlrichs, R. *Chem. Phys. Lett.* **1995**, *240*, 283−89.

(20) Ahlrichs, R.; Bär, M.; Häser, M.; Horn, H.; Kölmel, C. *Chem. Phys. Lett.* **1989**, *162*, 165−69.

(21) Frisch, M. J.; Trucks, G. W.; Schlegel, H. B.; Scuseria, G. E.; Robb, M. A.; Cheeseman, J. R.; Scalmani, G.; Barone, V.; Mennucci, B.; Petersson, G. A.; Nakatsuji, H.; Caricato, M.; Li, X.; Hratchian, H. P.; Izmaylov, A. F.; Bloino, J.; Zheng, G.; Sonnenberg, J. L.; Hada, M.; Ehara, M.; Toyota, K.; Fukuda, R.; Hasegawa, J.; Ishida, M.; Nakajima, T.; Honda, Y.; Kitao, O.; Nakai, H.; Vreven, T.; Montgomery, J. A., Jr.; ; Peralta, J. E.; Ogliaro, F.; Bearpark, M.; Heyd, J. J.; Brothers, E.; Kudin, K. N.; Staroverov, V. N.; Kobayashi, R.; Normand, J.; Raghavachari, K.; Rendell, A.; Burant, J. C.; Iyengar, S. S.; Tomasi, J.; Cossi, M.; Rega, N.; Millam, M. J.; Klene, M.; Knox, J. E.; Cross, J. B.; Bakken, V.; Adamo, C.; Jaramillo, J.; Gomperts, R.; Stratmann, R. E.; Yazyev, O.; Austin, A. J.; Cammi, R.; Pomelli, C.; Ochterski, J. W.; Martin, R. L.; Morokuma, K.; Zakrzewski, V. G.; Voth, G. A.; Salvador, P.; Dannenberg, J. J.; Dapprich, S.; Daniels, A. D.; Farkas, Ö.;

DOI: 10.1021/acs.joc.5b00243
J. Org. Chem. 2015, 80, 3921−3928

Foresman, J. B.; Ortiz, J. V.; Cioslowski, J.; Fox, D. J. *Gaussian 09; Revision D.01*; Gaussian, Inc., Wallingford, CT, 2009.

DOI: 10.1021/acs.joc.5b00243
J. Org. Chem. 2015, 80, 3921−3928